Polymers for Advanced Technologies

WILEY

polymers for advanced technologies

RESEARCH ARTICLE

Critical Parameters for the Properties of Poly (L-Lactic Acid) Mixed-Braided Stent: Monofilaments Diameter and Friction Coefficient

Jie Cheng[1] | Zhijie Jiang[1] | Xue Hu[1] | Muqing Liu[1] | Mingxi Lu[2] | Zhonghua Ni[1] | Gutian Zhao[1]

[1]School of Mechanical Engineering, Jiangsu Key Laboratory for Design and Manufacture of Micro-Nano Biomedical Instruments, Southeast University, Nanjing, China | [2]Undergraduate College of Literature, Science and the Arts, University of Michigan, Ann Arbor, Michigan, USA

Correspondence: Zhonghua Ni (zhaogutian@seu.edu.cn) | Gutian Zhao (zhaogutian@seu.edu.cn)

Received: 30 September 2024 | **Revised:** 3 December 2024 | **Accepted:** 4 December 2024

Funding: This study was supported by the National Key Research and Development Program of China (2023YFC3010301).

Keywords: braided stent | mixed-braided stent | poly (L-lactic acid) | radial supporting performance

ABSTRACT

Balancing the ideal radial supporting performance with flexibility in polymer stents has always been a significant challenge, and a potential solution to which is provided by the mixed-braided stents. However, the principles of mechanics and design advantages are yet ambiguous. This study aims to establish a correlation between radial supporting performance and structural morphologies of mixed-braided stents in the compression process. First, this study establishes a computational framework, which takes into account the different material properties of thick and thin monofilaments as well as actual friction coefficients. Second, this study simulates the crimping process of different mixed-braided stents to find out the relationship between radial supporting performance and structural morphologies. Finally, by changing the friction coefficient in the simulation model, the influence of friction coefficient on the crimping process of the stents is explored. The result provides a reference for the structural design of mixed-braided stents: significant differences in diameter and friction coefficient can lead to the instability of the stent. Specifically, as the friction coefficient increases from 0.12 to 0.20, the radial stiffness increases from 0.32 to 0.69 N/mm^2, which is an increase of 115%. However, the stability of the stent decreases simultaneously. Meanwhile, the COF and stability of the stent have declined.

1 | Introduction

Braided stents, characterized for exceptional flexibility and extensive applicability, have secured an important role within the realm of endovascular implantation. Benefitted from distinctive braided structure, braided stents demonstrate extraordinary flexibility, capable of freely conforming to the natural curvature of blood vessels [1–3]. It substantially diminishes the potential for endothelial injury, and consequently amplifies the likelihood of successful surgical outcomes. Furthermore, braided stents provide an extensive array of applications. Beyond their utility in addressing coronary artery diseases, they are also extensively utilized in the management of various intricate vascular conditions, including peripheral vascular diseases, carotid artery stenosis, and intracranial aneurysms [4, 5]. Therefore, the research and application prospects of braided stents are receiving considerable attention.

Depending on the material, braided stents can be divided into metal and polymer braided stents. Metal braided stents, usually braided from metal wires such as nickel–titanium alloy, stainless steel, or cobalt chromium alloy, have excellent mechanical properties and durability [6–8]. It is particularly suitable for the treatment of lesions that require long-term vascular support. However, with

© 2024 John Wiley & Sons Ltd.

the increasing clinical application of metal braided stents, their potential defects are gradually becoming apparent. Metal braided stents may induce chronic inflammation due to their permanent retention in the patient's body [9, 10]. These reactions may lead to intimal hyperplasia of blood vessels, thereby increasing the risk of in-stent restenosis (ISR) [11, 12]. Meanwhile, the metal wires of the metal braided stent may lead to vascular blockage, causing moderate or even severe complications such as myocardial infarction or stroke [13]. So, people are beginning to seek new treatment methods to avoid such defects. The development of bioabsorbable materials brings new choices for braided stents [14]. As a material for braided stents, bioabsorbable polymer materials have series of significant advantages, including good biocompatibility, comparably short-term retention in human body, and reduced risk of restenosis [15–19]. These characteristics bring bioabsorbable polymer braided stents academic prospects.

Poly (L-lactic acid) (PLLA) is a typical bioabsorbable material with good biocompatibility, which has been approved as a biomaterial implant by the US Food and Drug Administration [20]. It can be processed into PLLA monofilaments through methods such as melt extrusion and solid-state drawing [21], and these monofilaments exhibit superior mechanical properties, especially in withstanding compressive and bending forces [22]. PLLA braided stents can gradually be absorbed by the human body after serving their purpose in supporting blood vessels, helping to avoid a series of issues that may arise from the long-term implantation of metal stents, such as allergic reactions [23]. PLLA braided stents, while offering certain advantages, inherently possess the typical limitation associated with polymeric materials, notably a reduced radial supporting performance in comparison to their metallic counterparts. This relatively insufficient radial strength may limit the application of PLLA stents in the treatment of vascular lesions that require stronger vascular support, such as in larger blood vessels or where the vascular wall elasticity is poor. Therefore, to improve the shortcomings of the support strength of polymer stents, researchers have conducted many studies in this area. Liu et al. constrains the monofilament cross points in the stent by ultrasonic spraying process [24]. Similarly, Zhao et al. introduced axial runners into the stent design [15]. Although both of these modifications increased the radial supporting performance of the stent, unfortunately, they greatly compromised the flexibility of the stent and even led to the formation of kinks.

In previous studies, we proposed a mixed-braided stent composed of PLLA monofilaments with different stretching ratios. Through in-depth mechanical performance experiments on these mixed-braided stents, we found that the radial supporting performance of PLLA mixed-braided stents is similar to that of ordinary stents braided with thick diameters, and the flexibility of which is similar to that of ordinary stent braided with thin diameters [25]. It shows that PLLA mixed-braided stents can balance radial supporting performance and flexibility. In addition, compared with ordinary stents, the mixed-braided stents reduce the stent thickness, which minimize the impact on blood flow dynamics after implantation and mitigate negative issues such as thrombus accumulation. These open up a new path for the development of PLLA mixed-braided stents with excellent mechanical properties. However, although PLLA mixed-braided stents have shown potential, a deeper understanding of their mechanical properties and design advantages still needs to be elucidated.

First, this study establishes a computational framework, which takes into account the different material properties of thick and thin monofilaments as well as their actual friction coefficients. Second, this study simulates the radial supporting performance of PLLA mixed-braided stents with different diameters by finite element method and compares it with previous experimental data to confirm the accuracy of the simulation model. Finally, this study investigates the influence of friction coefficient on radial supporting performance of the stent and structural morphologies in the compression process.

2 | Materials and Methods

2.1 | Material

The PLLA raw material is purchased from Evonik Industries (Essen, Germany). The number-average molecular weight (Mn) and polydispersity index (PDI) are 367 kDa and 1.46, respectively. PLLA powder is processed into monofilaments with diameters of 0.15 ± 0.02, 0.19 ± 0.02, and 0.31 ± 0.02 mm through melt extrusion and solid-state drawing [22, 26]. The monofilaments used in the experiment are self-made by the above method.

2.2 | Tensile Test

PLLA monofilaments of different diameters (0.15, 0.19, and 0.31 mm) are used for series of tensile tests to obtain stress–strain curves as material parameters for finite element analysis. Tests are conducted with loading speed of 10 mm/min at room temperature by a self-made tensile testing machine. The stress–strain curves are shown in Figure 1a and material properties for monofilaments are depicted in Table 1.

2.3 | Friction Test

Unlike metal stents, the radial force of polymer stents is significantly influenced by friction [27]. Self-made friction testing machine based on Goksoy's proposed line contact method is used for testing the friction coefficient between monofilaments of different diameters, which aims to simulate actual situations accurately in finite element analysis. Tests are conducted with motor speed of 40 r/min and friction speed of monofilaments reaching 4.5 mm/s. The experimentally measured friction coefficient for the 0.15–0.31 monofilament is 0.122, and for the 0.19–0.31 monofilament, it is 0.119. The difference between the two is not significant, so we have uniformly set them to 0.12 in Abaqus.

2.4 | Radial Force Simulation

2.4.1 | Geometry and Material Model

Geometric models of PLLA mixed-braided stents are established by SolidWorks and imported into Abaqus CAE. One stent is woven by six monofilaments with diameters of 0.15 and 0.31 mm.

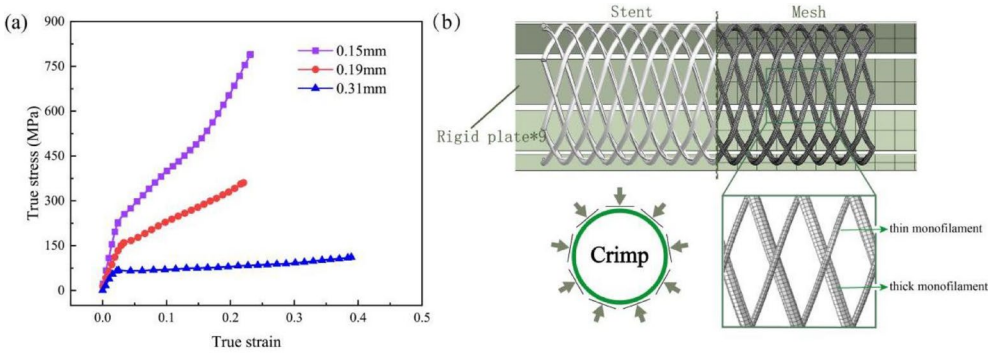


FIGURE 1 | (a) Stress–strain curves of monofilaments with different diameters. (b) Model diagram of finite element analysis.

TABLE 1 | Material properties for monofilaments.

Diameter (mm)	Young's modulus (GPa)	Yield strength (MPa)
0.15	8.9	247
0.19	4.9	121
0.31	3.7	55

Another one is woven by six monofilaments with diameters of 0.19 and 0.31 mm. The parameters of mixed-braided stents are shown in Table 2. The stents are modeled as an elastic–plastic material with Young's modulus of 8.9, 4.9, and 3.7 GPa, respectively, shown in Table 1. The Poisson's ratio of the stent is 0.3. The crimping tool is modeled as nine rigid plates distributed circumferentially around the stent geometry.

2.4.2 | Finite Element Model

The PLLA mixed-braided stent finite element model is shown in Figure 1b. The process of radial force simulation is divided into three steps, which are the crimping, holding, and expanding of the stents. Stents are crimped from the initial diameter to a diameter of 4 mm. The stent crimping simulation is a challenging non-linear quasi-static problem involving complex contact conditions. Therefore, Abaqus/Explicit is being used as a solver in this study. The modeling strategy is to implement a general contact interaction. This method has the advantage of being easy to define even for complex topologies and can be defined automatically for both rigid and deformable bodies. The friction formula adopts penalty friction, and the friction coefficient is set to 0.12 from friction tests. During the simulation process, displacement boundary conditions are applied to nine rigid plates, and no constraints are set for the stent. The stents are meshed using a linear hexahedral subtractive integral (C3D8R) element. The crimping tool is meshed using four-node three-dimensional bilinear rigid quadrilateral (R3D4) element. To compare different mixed-braided stent's radial supporting performance, this study shows radial stiffness and chronic outward force (COF) at 6 mm of stent. The radial stiffness equals the absolute value of the slope in the initial linear region of the radial force curve. The COF is obtained according to the ASTM F3067-14 standard under the intended use diameter (IUD) [28]. COF is defined as the radial expansion force between the IUD [25]. It reflects the ability of the stent to expand the blood vessel outwards.

2.5 | Radial Force Test

The radial force of the stent is tested using the American Blockwise TTR2 type radial force tester. The working temperature of the lumen is set to 37°C, and the stent is preheated in the lumen for 3 min before testing. During the compression phase, the stent is compressed from its initial outer diameter to 4 mm at a loading rate of 0.02 mm/s; during the stress relaxation phase, the stent is held static at 4 mm for 3 min without any change in deformation; during the expansion phase, the stent expands outwards at a loading rate of 0.02 mm/s. Prepare three stents for each set of parameters to conduct repeated experiments. The experimental data comes from previous research conducted in the laboratory [25].

3 | Results and Discussion

3.1 | Radial Supporting Performance

Radial force curves of PLLA mixed-braided stents are shown in Figure 2a. The 1, 2, and 3 in Figure 2a represent the crimping stage, holding stage, and expanding stage of the stent, respectively. The results indicate that there is a significant consistency between simulation and experimental data in the trend of radial force variation. The experimental values [25] for 0.15–0.31 and 0.19–0.31 stents are higher than the simulated values in Stage 1, with maximum errors of approximately 15% and 20%, respectively. This does not affect the consistency of the overall trend and can be partially attributed to the idealized assumption of the simulation model. The structure and material properties of the stent in the simulation model are assumed to be uniform and defect-free, while there may be material non-uniformity or slight deviations in the actual manufacturing process of the stent. In Stage 3, the radial force curves of the two stents intersect when the diameters of the stents are between 5.5 and 6 mm. When the diameter ranges from 4 to 5.5 mm, the radial force of the 0.15–0.31 stent is greater than the 0.19–0.31 stent. When the diameter is greater than 6 mm, this situation is reversed. Both simulation and experimental results show the above phenomenon. This further validates the reliability of the model.

Figure 2b shows the radial stiffness and COF at 6 mm of stents. For radial stiffness, there is a high degree of consistency between experimental and simulation values. For the COF at 6 mm, there is a certain difference between the simulation and experimental values for both stents, and these two differences are only 4.2% apart. Additionally, all simulation processes in this study are quasi-static, with the ratio of kinetic energy to internal energy being less than 5%.

3.2 | Relationship Between Radial Supporting Performance and Structural Morphology

Figure 3 shows the structural morphologies of the compression process for S-0.15-0.31 and S-0.19-0.31 stents. An important phenomenon is revealed by partial enlarged image: when stent of 0.19–0.31 is compressed to a diameter of 7.5 mm, the thin monofilaments show a certain degree of deviation relative to the thick monofilaments. This deviation gradually increases until it reaches its peak when compression is completed. The deviation of the thin monofilaments is greater in the same compression diameter for stent of 0.15–0.31.

This phenomenon may lead to a conclusion: Structure stability can be improved in stent design when the diameter of the thin monofilaments approaches that of the thick monofilaments. According to our previous research, the thin monofilaments in the mixed-braided stent can increase the flexibility [25]. Therefore, the diameter difference between the thick and thin monofilaments in the mix-braided stent should be maintained within a reasonable

TABLE 2 | Physical parameters of PLLA mixed-braided stents.

Stent label	Length (mm)	Internal diameter (mm)	External diameter (mm)	Braiding angle
E/S-0.15-0.31	20	8	8.92	17.12°
E/S-0.19-0.31	20	8	9	17.12°

Note: E represents experiment and S represents simulation.

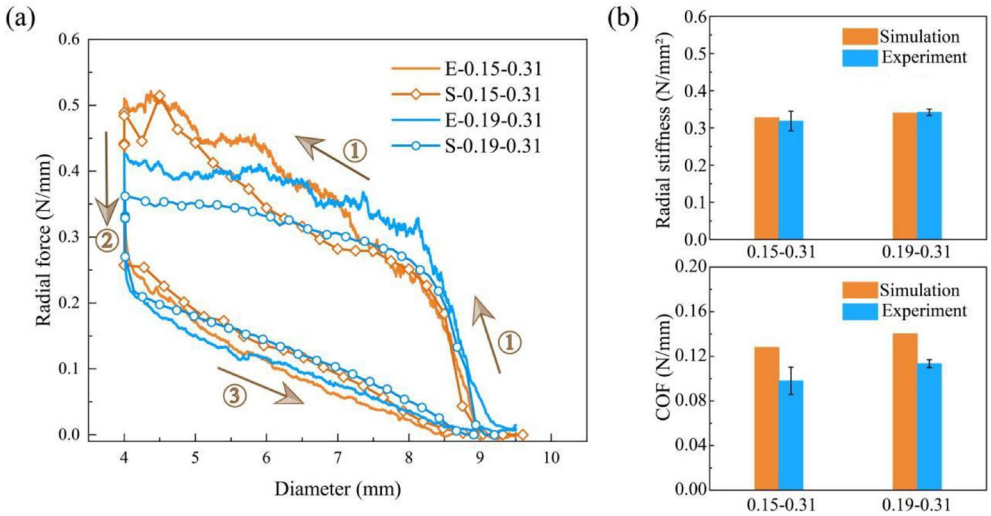


FIGURE 2 | Comparison between simulation and experiment of mixed-braided stents of 0.15–0.31 and 0.19–0.31: (a) Radial force curves. (b) Radial stiffness and COF at 6 mm.

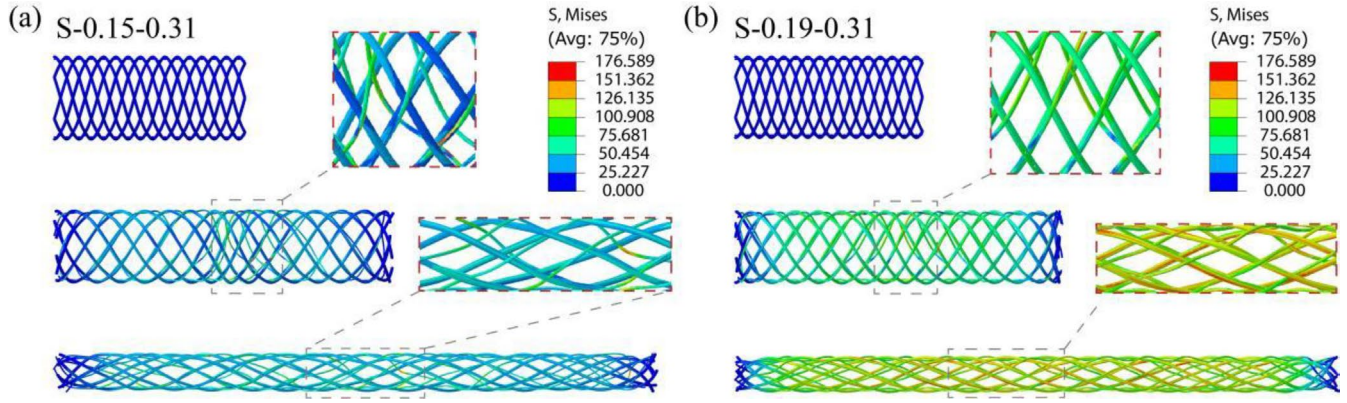


FIGURE 3 | Structural morphologies of the mixed-braided stents at initial diameter, 7.5 mm diameter, and complete compression: (a) S-0.15-0.31 and (b) S-0.19-0.31.

range. Meanwhile, this phenomenon can be further understood by associating with the radial force curve. The S-0.19-0.31 stent exhibits higher radial forces than the S-0.15-0.31 stent in the early stage of compression. It shows that thick monofilaments can provide strong radial force in stage of structure stability. However, the situation reversed in the later stages of compression. The radial force of the S-0.15-0.31 stent begins to exceed the S-0.19-0.31 stent and reaches the maximum difference when fully compressed. This change may be due to a decrease in the stability of the stent structure. At this point, the radial force is mainly determined by the interaction between monofilaments. Due to the more significant displacement of 0.15 mm monofilaments in the later stage of compression compared to 0.19 mm monofilaments, the interaction between 0.15 mm monofilaments and 0.31 mm monofilaments is more intense. As a result, a greater radial force is generated in the later stage of compression.

Von Mises stress cloud map and stress distribution bar chart of thick and thin monofilaments when fully compression mixed-braided stents with different diameters are shown in Figure 4.

As shown in Figure 4a,b, the thick monofilaments with 0.31 mm diameter can maintain stable spiral structure after being compressed in both types of mixed-braided stents. It is worth noting that there is a significant stress concentration phenomenon in some areas of the thick monofilament in the 0.19–0.31 stent, while no such problem was observed in the 0.15–0.31 stent. However, there is a significant difference in the performance of thin monofilaments compared to thick monofilaments. The thin monofilament can maintain spiral shape in the 0.19–0.31 stent. In the 0.15–0.31 stent, the structure of the thin monofilament has twisted. The maximum stress of both stents happens to appear on the thin monofilaments. The maximum stress on a 0.15 mm monofilament is 176 MPa, which is much greater than the 58 MPa on a 0.19 mm monofilament. However, large stress concentration should be avoided as it may affect the overall performance of the stent and make the deformation process of the stent unpredictable.

Figure 4c,d supplements Figure 4a,b, showing the stress distribution of thick and thin monofilaments in the mixed-braided

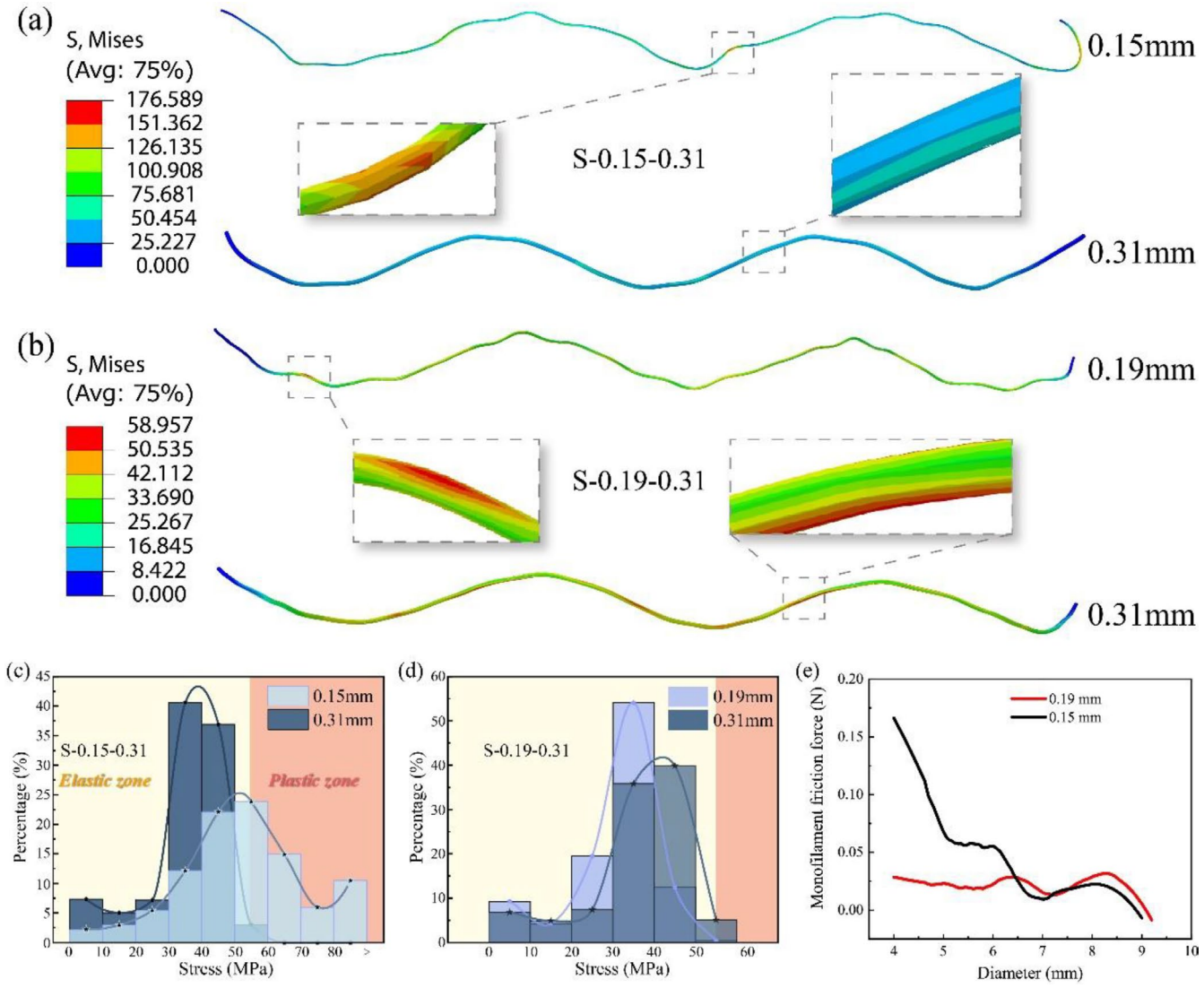


FIGURE 4 | Von Mises stress cloud map and stress distribution bar chart of thick and thin monofilaments when fully compression mixed-braided stents with different diameters: (a) S-0.15-0.31, (b) S-0.19-0.31, and (c) S-0.15-0.31. The last bar in the figure represents stress above 80 MPa. (d) S-0.19-0.31. (e) The frictional force of individual thin monofilament in different mixed-braided stents.

stents. The color backgrounds represent the elastic and plastic regions of the 0.31 mm monofilament, which are derived from the yield strength of the monofilament. The study focuses on the elastic–plastic region of the 0.31 mm monofilament because it has the lowest yield strength and is more susceptible to plastic strain. From the figure, the stress distribution range of 0.31 mm monofilaments is roughly the same and mainly located in the elastic region in stents. Based on previous research, the deformation of monofilament should be limited in elastic zone; otherwise, the structure could turn disordered with stress concentration and plastic deformation, which may lead to unpredictable mechanical performance [29]. In addition, the stress distribution of the 0.31 mm monofilaments shows a common characteristic: 75% of the stress area is located in the stress range of 30–50 MPa. For the 0.19 mm monofilament, the stress distribution area approximates the 0.31 mm monofilament, which is 0–60 MPa. Meanwhile, about 55% of the stress area is located in the stress range of 30–40 MPa. This shows that the stress distribution of the thick and thin monofilaments is relatively uniform, which is conducive to maintaining the stability of the support. The stress distribution of 0.15 mm monofilament significantly differs from that of 0.19 mm monofilament. The stress of 0.15 mm monofilament is widely distributed, with a maximum stress of 176 MPa. Meanwhile, only 10% of the area with stress exceeds 80 MPa in 0.15 mm monofilament. This indicates that 0.15 mm monofilament has stronger concentrated stress, which may be related to the irregular twisting deformation of 0.15 mm monofilament. It is detrimental to the stability of the stent structure, which can make the behavior of the stent unpredictable. In addition, about 60% of the stress area is located in the stress range of 40–70 MPa. This stress area exceeds the 30–40 MPa stress area of 0.19 mm monofilament.

We reflect the interaction between monofilaments by extracting the frictional force exerted on single monofilament. The greater the frictional force, the more intense the interaction, which also implies an increase in the radial force of the stent.

Figure 4e reveals the frictional forces experienced by single thin monofilament in different mixed-braided stents. In the early stages of compression, as the diameter of the stent decreases, the frictional forces experienced by the thin monofilament in both types of stents increase, with the 0.19 mm monofilament experiencing slightly more friction than the 0.15 mm monofilament. It is similar to the changes in the radial force of the stents. Subsequently, the frictional force on the 0.19 mm monofilament remains relatively stable, eventually reaching 0.029 N, while the frictional force on the 0.15 mm monofilament increases sharply in the later stages of compression, ultimately reaching 0.166 N, indicating a stronger interaction. Correspondingly, the radial force of the 0.15–0.31 stent in the later stages of compression exceeds the 0.19–0.31 stent.

As shown in Figure 5a, the 0.19–0.31 stent can maintain stable structure after expansion with uniform diamond-shaped regions and a 97% recoil rate. This is very beneficial for the clinical application of stents, as they can provide stable support, ensuring the reliability and persistence of treatment outcomes. In contrast, the 0.15–0.31 stent cannot maintain its original form after expansion, with irregularly shaped diamond areas and residual stress of 20–30 MPa in some areas. The central diamond-shaped regions are too small, while the ends are excessively large, and in some places, diamond-shaped regions can no longer be formed. The uniformity of the diamond-shaped areas is an important factor in observing whether the stent structure is stable. The aforementioned phenomenon indicates that the 0.15–0.31 stent cannot maintain a stable structure after expansion. Meanwhile, its resilience is poor, and the structure at the ends of the stent has become disordered. The plastic strain of the corresponding parts of the thick monofilaments in the two stents is shown in Figure 5b. The part taken from the diagram is the middle section of the monofilaments. In the 0.15–0.31 stent, the thick monofilament is slightly twisted, and plastic deformation occurs in the lower part of the monofilament. In contrast, the thick monofilament in the 0.19–0.31 stent is regular and there are no areas of plastic deformation. Similar situations are also observed in other thick monofilaments in both stents, and the maximum plastic strain of the thick monofilaments is found in the 0.15–0.31 stent. This may be an important factor leading to the poor appearance of the 0.15–0.31 stent after expansion. For 0.19–0.31 stent, the experimental and simulation results are largely consistent, both exhibiting good structural stability and resilience. However, for 0.15–0.31 stent, there is a certain discrepancy between the experimental and simulation structural morphologies. This discrepancy may stem from severe monofilament disorder during the crimping process, which reduces the predictability of the stent's behavior. In clinical applications, the structural stability and

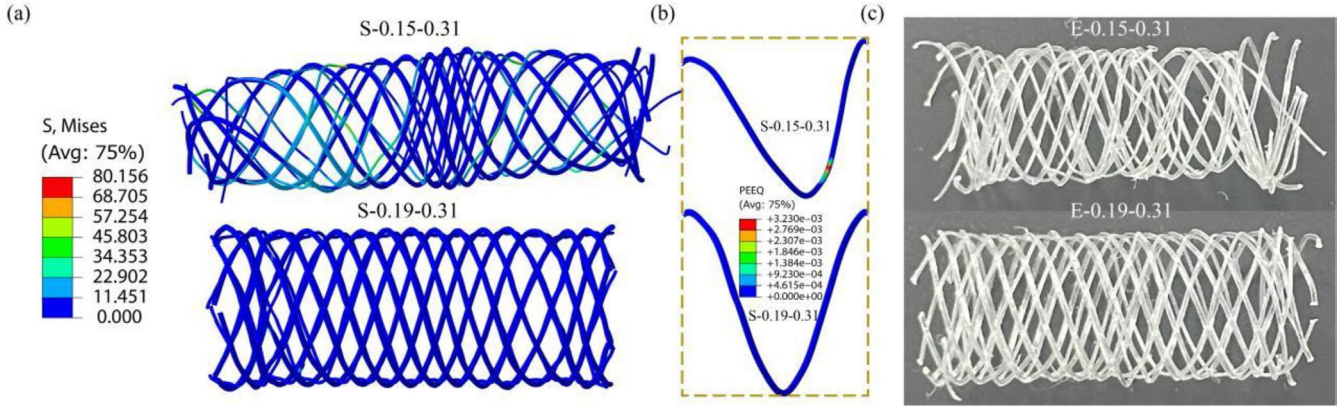


FIGURE 5 | (a) Von Mises stress cloud map after the expansion of the stents. (b) The partial plastic strain of the monofilaments after expansion. (c) The appearance of the stents after experimental expansion.

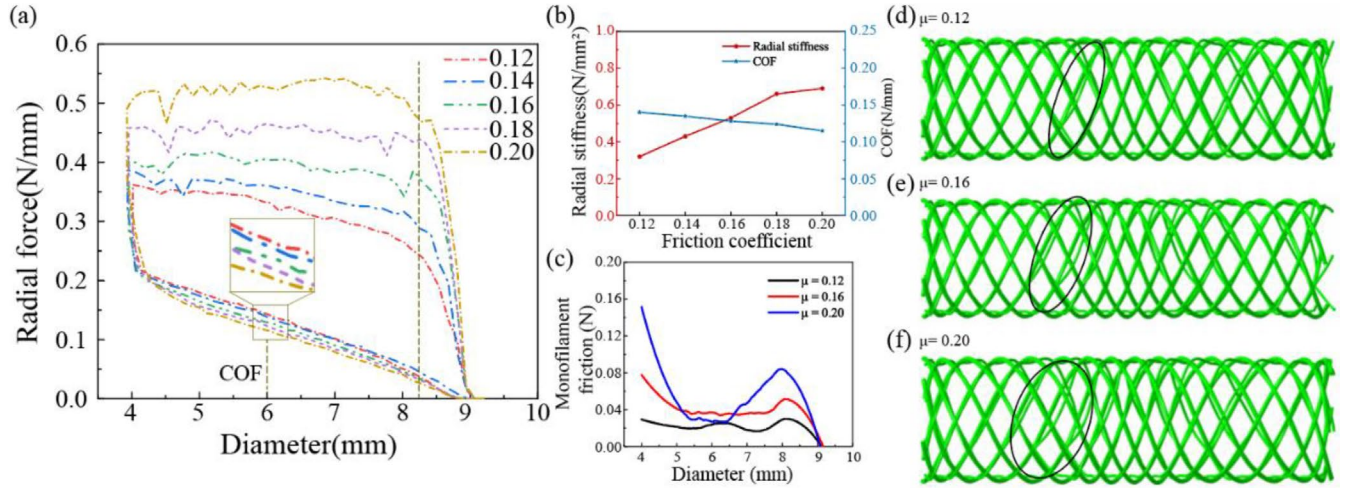


FIGURE 6 | (a) Radial force curves of 0.19–0.31 mixed-braided stent under different friction coefficients. (b) Comparison of radial stiffness and COF at 6 mm under different friction coefficients. (c) The frictional force of the thin monofilament in mixed-braided stent with different friction coefficients. (d–f) Structural morphologies of support at 8.25 mm under friction coefficients of 0.12, 0.16, and 0.20, respectively.

predictability of stents are crucial. Thus, excessive differences in monofilament diameters should be avoided in stent design. To ensure the safety and effectiveness of the stent, a compromise should be made between mechanical performance and structural stability.

3.3 | Impact of Friction Coefficient

To investigate the influence of friction coefficient on the radial force and structural morphology of the stent, multiple simulations are conducted by changing the friction coefficient in the simulation model. The influence of friction coefficient on structural morphologies and radial force of stent is shown in Figure 6. As shown in Figure 6a,b, with the increase of friction coefficient, the radial force and radial stiffness of the stent show an upward trend, while the COF shows a downward trend. Interestingly, as the friction coefficient increases, the radial stiffness of the stent and the COF increase and decrease in an approximately linear trend, with the radial stiffness being more significantly affected. When the friction coefficient is increased from 0.12 to 0.20, the radial stiffness increases from 0.32 to 0.69 N/mm^2, with a growth rate of 115%, while the COF only decreases by about 18%. Meanwhile, the vibration amplitude during the compression process also intensifies. The impact of this kind of friction on the mechanical performance parameters of the stent could be further studied in the future. The effect of different friction coefficients on the shape of the stent at a compression diameter of 8.25 mm is shown in Figure 6d–f. The results reveal a significant trend: as the friction coefficient increases, the deviation of the thin monofilaments relative to the thick monofilaments increases. This discovery indicates that the increase in friction coefficient strengthens the interaction between monofilaments, leading to an unstable local structure of the stent under the same compression diameter. The instability of this structure may be the fundamental reason for the increase in radial force. Therefore, more caution is needed for the surface treatment of monofilaments to prevent structural defects caused by excessive changes in friction.

Figure 6c demonstrates the frictional forces experienced by single thin monofilament in the 0.19–0.31 stent under various friction coefficients. As shown in Figure 3c, as the friction coefficient increases, the frictional forces on the thin monofilament also correspondingly increase, from an initial 0.029 N to a final 0.151 N. This is also a clear indication of interactions between the monofilaments.

4 | Conclusion

The diameter of monofilaments and coefficient friction have a significant impact on the radial supporting performance of PLLA mixed-braided stent. In this study, we establish a computational framework and simulate the crimping process of different mixed-braided stents to determine the relationship between radial supporting performance and structural morphologies. The result indicates that a significant difference in the diameter of thick and thin monofilaments can reduce the structural stability of the mixed-braided stent, making the deformation of the stent unpredictable. Therefore, the diameters of thick and thin monofilaments in the mixed-braided stent should be maintained within a reasonable range. This study provides a reference for the structural design of mixed-braided stents, and future research may further explore the optimal diameter difference between thick and thin monofilaments in mixed-braided stents. In addition, we investigate the influence of friction coefficient on radial force and structural morphology of the stent. The results indicate that an increase in friction coefficient will enhance the interaction between monofilaments, which will strengthen radial supporting performance. However, it will lead to unstable local structures of the stent under the compression. Therefore, more caution is needed when performing surface treatments of monofilaments to prevent structural defects caused by excessive changes in friction.

This study presents some limitations. This study investigates mixed-braided stents of different diameters and found that the diameters and the friction coefficient between the

monofilaments affect the mechanical properties and stability of the stent. However, it did not explore a range of values or provide guidance for the best parameters. The subsequent gradient increases the diameter of the thin monofilament for further discussion. In addition, the practical application of mixed-braided stents in biodegradable stents needs to be discussed. The different degradation rates of thick and thin monofilaments may affect the long-term structural integrity of the stent. Addressing this issue will enhance the clinical relevance of this study. The aforementioned issue will be further discussed in the subsequent research.

Acknowledgments

This paper was supported by the National Key R&D Program of China (2023YFC3010301).

Conflicts of Interest

The authors declare no conflicts of interest.

Data Availability Statement

The data that support the findings of this study are available from the corresponding author upon reasonable request.

References

1. K. Maleckis, P. Deegan, W. Poulson, et al., "Comparison of Femoropopliteal Artery Stents Under Axial and Radial Compression, Axial Tension, Bending, and Torsion Deformations," *Journal of the Mechanical Behavior of Biomedical Materials* 75 (2017): 160–168.

2. J. H. Kim, T. J. Kang, and W. R. Yu, "Mechanical Modeling of Self-Expandable Stent Fabricated Using Braiding Technology," *Journal of Biomechanics* 41 (2008): 3202–3212.

3. U. Sharma, D. Concagh, L. Core, et al., "The Development of Bioresorbable Composite Polymeric Implants With High Mechanical Strength," *Nature Materials* 17 (2018): 96–103.

4. T. M. Isotalo, J. P. Nuutine, A. Vaajanen, et al., "Biocompatibility Properties of a New Braided Biodegradable Urethral Stent: A Comparison With a Biodegradable Spiral and a Braided Metallic Stent in the Rabbit Urethra," *BJU International* 97 (2006): 856–859.

5. L. Moeri, M. Lichtenberg, S. Gnanapiragasam, S. Barco, and T. Sebastian, "Braided or Laser-Cut Self-Expanding Nitinol Stents for the Common Femoral Vein in Patients With Post-Thrombotic Syndrome," *Journal of Vascular Surgery. Venous and Lymphatic Disorders* 9 (2021): 760–769.

6. H. Guo, Y. He, Y. Zheng, and Y. Cui, "In Vitro Studies of Biodegradable Zn-0.1Li Alloy for Potential Esophageal Stent Application," *Materials Letters* 275 (2020): 128190.

7. T. Koizumi, H. Kaneda, S. Sakai, A. Sato, and K. Aonuma, "In Vivo Illustration of Dendrite Formation on a Mobile Thrombus Within a Wallstent in an Iliac Artery: A Fractal Phenomenon," *Annals of Vascular Diseases* 12 (2019): 103–104.

8. L. Capoccia, P. Sirignano, W. Mansour, et al., "Peri-Procedural Brain Lesions Prevention in CAS (3PCAS): Randomized Trial Comparing CGuard Stent vs Wallstent," *International Journal of Cardiology* 279 (2019): 148–153.

9. J. Li, Y. Zhang, Y. Qin, B. Xiao, and S. Wang, "Improvement of Cu and Zr Doped Diamond-Like Carbon Coatings on Comprehensive Performance of Ni-Ti Alloy Potentially Used in Braided Vascular Stent," *Thin Solid Films* 782 (2023): 140020.

10. L. L. Liu, J. Qin, C. H. Zeng, et al., "Biodegradable PTX-PLGA-Coated Magnesium Stent for Benign Esophageal Stricture: An Experimental Study," *Acta Biomaterialia* 146 (2022): 495–505.

11. X. Liu, H. Tao, C. Li, et al., "Effect of NiTi Parameters on the Mechanical Properties of Integrated Braided Stents," *Textile Research Journal* 93 (2022): 701–712.

12. R. V. Marrey, R. Burgermeister, R. B. Grishaber, and R. O. Ritchie, "Fatigue and Life Prediction for Cobalt-Chromium Stents: A Fracture Mechanics Analysis," *Biomaterials* 27 (2006): 1988–2000.

13. A. Lucchetti, C. Emonts, A. Idrissi, T. Gries, and T. J. Vaughan, "An Experimental Investigation of the Mechanical Performance of PLLA Wire-Braided Stents," *Journal of the Mechanical Behavior of Biomedical Materials* 138 (2023): 105568.

14. X. Hu, Q. Liu, L. Chen, et al., "Modified Theoretical Model Predicts Radial Support Capacity of Polymer Braided Stents," *Computer Methods and Programs in Biomedicine* 246 (2024): 108063.

15. F. Zhao, W. Xue, F. Wang, et al., "Braided Bioresorbable Cardiovascular Stents Mechanically Reinforced by Axial Runners," *Journal of the Mechanical Behavior of Biomedical Materials* 89 (2019): 19–32.

16. F. Zhao, J. Sun, W. Xue, et al., "Development of a Polycaprolactone/Poly(P-Dioxanone) Bioresorbable Stent With Mechanically Self-Reinforced Structure for Congenital Heart Disease Treatment," *Bioactive Materials* 6 (2021): 2969–2982.

17. Y. Liu, G. Zhu, H. Yang, C. Wang, P. Zhang, and G. Han, "Bending Behaviors of Fully Covered Biodegradable Polydioxanone Biliary Stent for Human Body by Finite Element Method," *Journal of the Mechanical Behavior of Biomedical Materials* 77 (2018): 157–163.

18. H. Jaziri, S. Mokhtar, Y. Kyosev, N. Chakfe, F. Heim, and S. Ben Abdessalem, "Influence of Fatigue Stress on the Radial Strength of Polymeric Braided Vascular Stents," *Polymers for Advanced Technologies* 33 (2021): 627–637.

19. H. Jaziri, S. Mokhtar, N. Chakfe, F. Heim, and S. B. Abdessalem, "Elastic Recovery of Polymeric Braided Stents Under Cyclic Loading: Preliminary Assessment," *Journal of the Mechanical Behavior of Biomedical Materials* 98 (2019): 131–136.

20. Y. Liu, J. Yang, Y. Zhou, and J. Hu, "Structure Design of Vascular Stents," in *Multiscale Simulations and Mechanics of Biological Materials* (Chichester, West Sussex, UK: John Wiley & Sons, Inc, 2013), 301–317.

21. C. M. Agrawal, K. F. Haas, D. A. Leopold, and H. G. Clark, "Evaluation of Poly(L-Lactic Acid) as a Material for Intravascular Polymeric Stents," *Biomaterials* 13, no. 3 (1992): 176–182.

22. G. Zhao, X. Li, Y. Tian, et al., "Poly(L-Lactic Acid) Monofilaments for Biodegradable Braided Self-Expanding Stent," *Journal of Materials Science* 56 (2021): 12383–12393.

23. M. Jamshidi, M. Rajabian, M. B. Avery, et al., "A Novel Self-Expanding Primarily Bioabsorbable Braided Flow-Diverting Stent for Aneurysms: Initial Safety Results," *Journal of NeuroInterventional Surgery* 12 (2020): 700–705.

24. W. T. Liu, B. Wang, X. Hu, J. Lv, and G. T. Zhao, "A Biodegradable Polymer Stent With High Radial Performance: Potential for Treatment of Portal Vein Stenosis," *Polymers for Advanced Technologies* 35 (2024): e6451.

25. M. Liu, Y. Tian, J. Cheng, Y. Zhang, G. Zhao, and Z. Ni, "Mixed-Braided Stent: An Effective Way to Improve Comprehensive Mechanical Properties of Poly (L-Lactic Acid) Self-Expandable Braided Stent," *Journal of the Mechanical Behavior of Biomedical Materials* 128 (2022): 105123.

26. X. Li, Y. Tian, J. Zhang, et al., "Effects of Annealing Constraint Methods on Poly(L-Lactic Acid) Monofilaments for Application in Stents Annealing," *Polymers for Advanced Technologies* 32 (2021): 2378–2385.

27. C. Zhang, X. Hu, B. Wang, et al., "Design Strategy of Poly (L-Lactic Acid) Mixed Braided Stent: The Influence of Braiding Ratio of Thick

and Thin Monofilaments," *Journal of Applied Polymer Science* 141 (2024): e55100.

28. F. Committee, *Guide for Radial Loading of Balloon Expandable and Self Expanding Vascular Stents* (West Conshohocken, PA: ASTM International, 2023).

29. J. Li, J. Cheng, X. Hu, et al., "A Hazardous Boundary of Poly(L-Lactic Acid) Braided Stent Design: Limited Elastic Deformability of Polymer Materials," *Journal of the Mechanical Behavior of Biomedical Materials* 138 (2023): 105628.